MM Science Journal | www.mmscience.eu
ISSN 1803-1269 (Print) | ISSN 1805-0476 (On-line)
Special Issue | HSM 2025
18th International Conference on High Speed Machining
October 15-16, 2025, Metz, France
DOI: 10.17973/MMSJ.2025_11_2025135

HSM2025-44815

NUMERICAL METHOD FOR DESIGNING A TWO-DIMENSIONAL DE LAVAL NOZZLE FOR OPTIMIZATION IN ASSISTED MACHINING WITH SUPERCRITICAL CO_2

T. Gosset[1,2]*, M. Deligant[3], F. Rossi[1], G. Poulachon[1], R. M'Saoubi[4], S. Arsene[5]

[1]Arts et Metiers Institute of Technology, LaBoMaP, F-71250 Cluny, France

[2]R&D Milling and Process Seco Tools AB, F-18020 Bourges, France

[3]Arts et Metiers Institute of Technology, CNAM, LIFSE, F-75013 Paris, France

[4]R&D Material and Technology Development Seco Tools Ab, SE-73782 Fagersta, Sweden

[5]Constellium Technology Center; 725 rue Aristide Berges, Centr'Alp, F-38341 Voreppe, France

*Corresponding author; e-mail: thomas.gosset@ensam.eu

Abstract
The purpose of this work is to present a quick method for designing the divergent section of planar Laval micro-nozzles in order to predict the properties of the CO_2 jet at the nozzle and better control the cooling effect in the context of cryogenic machining with supercritical CO_2 ($ScCO_2$). The Method of Characteristics (MOC) and a real gas model have been implemented to obtain 2D nozzles divergent part adapted for single-phase gas expansion. CO_2 inlet pressure, inlet temperature, and pressure distribution along the nozzle axis are set as input parameters. A 2D nozzle facility has been developed to allow visualization of the CO_2 jet and its expansion in ambient air. Preliminary results are presented to demonstrate the potential of the facility.

Keywords:
Supercritical, CO2, nozzle expansion, Method of Characteristics, assisted machining

1 INTRODUCTION

Recycling aluminium chips is a critical issue in the manufacturing of integrally-machined aeronautical structural parts (with a buy/fly ratio of up to 20). Due to the stringent requirements for part quality and safety standards, cutting fluids are commonly used, polluting the chips and thereby increasing the cost and energy consumption of the remelting process [Altharan 2024]. For certain alloys, such as aluminium-lithium alloy 2050-T84, chip recycling is very restrictive due to the low pollution levels that must be achieved and the strict methods that must be implemented for these alloys [Riquet 2011].

Moreover, the aeronautical market is driven by a steady increase in air traffic despite the COVID crisis. According to analyses by the International Air Transport Association [IATA 2022], the crisis had a profound effect on air transport, reducing the number of annual passengers from 4 billion to 1.5 billion between 2019 and 2020. However, in just 5 years, the sector has bounced back, reaching the same level of civil air traffic in 2024 as in 2019. IATA also forecasts an average annual increase in air traffic of +3.3%, taking total passenger traffic to 8 billion per year in 2040, doubling the current level.
To meet this demand, the aviation sector must not only increase its overall fleet of aircraft but also replace a large proportion of it in order to achieve the carbon neutrality targets set by the International Civil Aviation Organization by 2050.
Thus, the use of new emerging machining assistance, such as supercritical CO_2 ($ScCO_2$) could reduce or eliminate the need for cutting fluids, produce clean chips, and contribute to carbon emission reduction. This technology could also increase tool life and productivity, but its cooling power is still poorly understood.

1.1 Supercritical CO_2 in machining

$ScCO_2$ is a fluid state that can be achieved when CO_2 is maintained above a critical pressure and a critical temperature (approximately $74\ bar$ and $31\ °C$). In this state, CO_2 is considered a 'super-solvent' and can uniformly dissolve small quantities of oils and lubricants [Clarens 2006].

Compared to conventional cryogenic assistance processes that deliver a medium at cryogenic temperature, such as liquid LN_2, the cooling effect is produced by adiabatic expansion of the fluid through the nozzle, known as Joule-Thomson expansion [Proud 2022]. The jet projected onto the cutting zone is a mixture of gas that can reach a temperature of approximately $-80\ °C$ (solidification of CO_2 at atmospheric pressure) and dry ice. Most studies agree that $ScCO_2$ decreases the temperature around the cutting edge during the process [Gao 2024] [Huang 2022]. Combining $ScCO_2$ with Minimum Quantity Lubrication

(MQL) increases tool life and reduces cutting forces, which is not always the case when using $ScCO_2$ without any lubricant [Cai 2021] [Tapoglou 2021].

1.2 Effect of nozzle geometry on CO_2 jet structure and cooling effect

In the literature, no studies focus directly on the influence of nozzle geometry on CO_2 jet structure and cooling ability in the context of machining with $ScCO_2$ assistance. Some research mentions simple modifications of straight nozzle outlet diameter to change the CO_2 mass flow rate and observe its influence on tool life and type of wear.

[Proud 2023] employed mass flow rates of $250\ g/min$, $583.3\ g/min$, and $916.6\ g/min$ for sapphire nozzles with respective diameters of $0.2\ mm$, $0.4\ mm$, and $0.6\ mm$, at a CO_2 pressure of $138\ bar$ for shoulder milling of grade 2 commercially pure titanium. For certain cutting speed conditions, an increase of mass flow rate results in a reduction of tool life due to a potential overcooling modifying the material's properties. [Stephenson 2014] employed mass flow rates of $280\ g/min$ and $450\ g/min$ for nozzles with respective diameters $0.25\ mm$ and $0.34\ mm$, $165\ bar$ and $40°C$ for rough turning Inconel 750 with MQL dissolution. The optimal flow rate required was $70\ g/min$ of CO_2 per kW of cutting power. However, no variations in $ScCO_2$ pressure and temperature were tested, which could have a significant impact on the cooling effect.

The investigation of CO_2 phase proportions (gas, liquid, solid, metastable) and fluid properties during flow expansion is poorly explored in machining areas. They are more commonly discussed through topics related to CO_2 capture or the optimization of supercritical carbon dioxide power cycle systems by studying De Laval nozzle geometries [Lettieri 2018].

This preliminary work aims to develop a shape optimization program in Python for divergent section of convergent-divergent (C-D) nozzles, with the objective of controlling the expansion of supercritical CO_2 in the context of cryogenic-assisted machining. The main parameters targeted at the nozzle outlet are temperature (as low as possible) and pressure and velocity, with the objective of ultimately controlling the phase change of CO_2 during expansion and heat transfer on the tool/chip area. A dedicated 2D flow study cell has been designed to analyze the effects of various nozzle geometries on the expansion dynamics. Preliminary tests will be presented.

Nomenclature

Thermodynamic variables

h specific enthalpy (J/kg)
s specific entropy (J/kg)
p pressure (MPa)
ρ density (kg/m^3)
a speed of sound (m/s)
T temperature (K)
$\dot{m}$ mass flow rate (kg/m/s)
γ heat capacity ratio

Kinematic variables

u velocity compound along x
v velocity compound along y
V velocity magnitude
M Mach number

Geometrical variables

φ local flow angle
α Mach angle
R radius of curvature of the throat wall
H_t Semi-height of the throat
ξ Characteristic line

Localization index

$_0$ inlet
$_t$ throat
$_e$ exit

Other

$\bar{w}$ normalization of w variable

2 NOZZLE SHAPE COMPUTATION

2.1 Convergent-divergent nozzle

A convergent-divergent (C-D) nozzle, also known as a De Laval nozzle, is a duct designed to accelerate a hot, pressurized fluid to supersonic speeds. The thermal energy present upstream of the nozzle is thereby converted into kinetic energy. This change in fluid velocity is commonly expressed in dimensionless form as the Mach number M defined by (1):

$$M = \frac{V}{a} \tag{1}$$

Fig.1 shows a typical evolution of a flow across a C-D nozzle, temperature and pressure along the nozzle axis and the subsonic, sonic, and supersonic domains associated with the Mach number value.

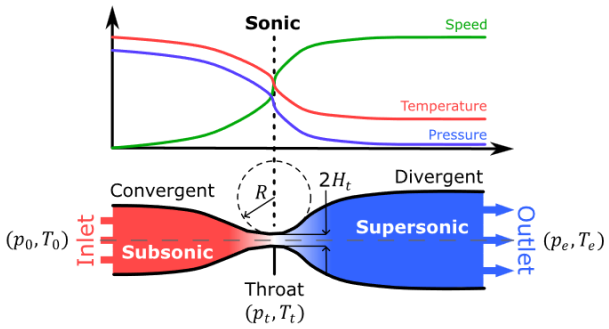

Fig. 1: Evolution of thermodynamic and kinetic properties along a nozzle axis

In the converging section, the flow is assumed to have a preservation both of total enthalpy h_0 and total pressure p_0, while in the divergent section, it undergoes an isentropic expansion with conservation of total enthalpy. For a first approach, the flow is assumed to be inviscid (neglecting viscosity and boundary layers), adiabatic, and shock-free.

2.2 Methodology

The input parameters required to initiate the design procedure are upstream total pressure p_0 and upstream total temperature T_0 of CO_2 in the supercritical area, exit pressure p_e, and throat semi-height H_t (see Fig.1).

The calculation procedure is implemented as follows and will be detailed in the following sections:

- Calculation of thermodynamic properties at the throat, mass flow rate $\dot{m}$ and pressure evolution along the nozzle axis $p(x)$.
- Selection of transonic domain model.
- Selection of solver method between Method of Characteristics (MOC) for Ideal gas, MOC for Equivalent gas (EGM) or Advanced Gas Model (AGM)
- Solving governing equations.
- Determination of nozzle geometry by maintaining flow rate.

The next sections expand on each point of the method.

The methodology is based on the design work of the supersonic stator of [Bufi 2016], and is supported by the work of [Délery 2010].

2.3 Governing equation

The flow is considered steady and irrotational in the divergent section of the nozzle. The flow is governed by the 2D isentropic Euler equations and can be described by two families of characteristic lines (2) and (3):

$$\frac{dy}{dx} = \tan(\varphi \pm \alpha) \qquad (+ \Rightarrow left - r; - \Rightarrow right - r) \qquad (2)$$

$$d\varphi \pm \sqrt{M^2 - 1}\frac{dV}{V} = 0 \quad (- \Rightarrow left - r; + \Rightarrow right - r) \qquad (3)$$

$$\varphi \pm \nu(M, \gamma) = cst \quad (- \Rightarrow left - r; + \Rightarrow right - r) \qquad (4)$$

$$\nu(M, \gamma) = \sqrt{\frac{\gamma+1}{\gamma-1}}\tan^{-1}\sqrt{\frac{\gamma-1}{(\gamma+1)(M^2-1)}} - \tan^{-1}\sqrt{M^2 - 1} \qquad (5)$$

$\alpha = \arcsin(M^{-1})$ is the Mach angle. (4) is an analytical integration of (3) for a perfect gas. The signs + and – are associated with right-running and left-running characteristic lines. φ, α, and the characteristic lines are represented on Fig. 2. (5) is the Prandtl-Meyer function and describes the angle through which a supersonic flow must turn to reach a given Mach number. (2) and (3) constitute the governing equations for the Advanced Gas Model, and (2) and (4) for MOC.

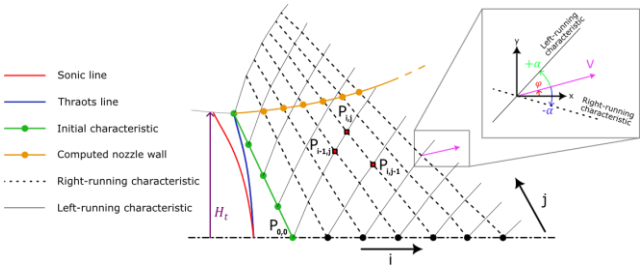

Fig. 2: Calculation patterns of divergent nozzle section. Here, the first six points of the nozzle wall are drawn

2.4 Throat thermodynamic properties

Between the inlet and the nozzle throat, CO_2 evolves assuming a preservation of total enthalpy and total pressure; the following equations can be extracted:

$$h_t = h_0(p_0, T_0) - \frac{V_t^2}{2} \qquad (6)$$

$$p_t = p_0 - \rho_t \frac{V_t^2}{2} \qquad (7)$$

h_0 can be determined by using the open-source Python thermodynamic library CoolProp [Bell 2014]. Knowing that the flow at the throat is sonic, (1) can be rearranged to obtain the condition of equation (8):

$$f(V_t - a_t) = V_t - a_t = 0 \qquad (8)$$

(6), (7), and (8) can be combined into a nonlinear equation integrating CoolProp evaluation of a_t and ρ_t. The throat entropy $s_t(p_t, h_t)$ is then determined with CoolProp for the isentropic expansion.

The mass flow rate at the throat is then calculated with (9):

$$\dot{m}_t = a_t \cdot 2H_t.\rho_t \qquad (9)$$

The pressure evolution along the nozzle axis is defined with a cubic distribution (10) between the throat and the outlet to have a smooth acceleration:

$$p(x) = p_t + (p_e - p_t) \cdot \left(\frac{x-L}{x}\right)^3 \qquad (10)$$

L is a characteristic length of pressure relaxation and is set to $10H_t$ to avoid overlapping characteristic lines, and to avoid the formation of internal shocks [Délery 2010].

2.5 Transonic domain model

According to [Délery 2010], the normalized governing equation of the transonic domain is given by (11):

$$[\bar{a}^2 - (\bar{u})^2]\frac{\bar{u}}{\partial \bar{x}} + [\bar{a}^2 - (\bar{v})^2]\frac{\bar{v}}{\partial \bar{y}} - 2\bar{u}\bar{v}\left(\frac{\bar{u}}{\partial \bar{x}}\frac{\bar{v}}{\partial \bar{y}}\right) = 0 \qquad (11)$$

$\bar{a}$, $\bar{u}$, and $\bar{v}$ are normalized with respect to the critical speed of sound a_t, $\bar{x} = \beta x$ and $\bar{y} = \beta y$. β is a factor between the non-dimensional system and the dimensional system, which will be defined later.

Several methodologies exist to solve (11), such as the Sauer's Method [Délery 2010]. Here, $\bar{u}(\bar{x}, \bar{y}, \gamma)$ and $\bar{v}(\bar{x}, \bar{y}, \gamma)$ come from [Bufi 2016], applying the Carrière's method [Délery 2010]. The calculations required to obtain them are complex. They are not described here but will be used to initialize the MOC and the AGM.

Mach number is evaluated as:

$$M = \sqrt{\frac{\bar{u}^2 + \bar{v}^2}{\frac{\gamma+1}{2} - \frac{\gamma-1}{2}(\bar{u}^2 + \bar{v}^2)}} \qquad (12)$$

2.6 Method of Characteristics for Ideal Gas

Initial characteristic ξ_0

To apply the MOC, a right-running initial characteristic ξ_0 linking the wall of the throat and the nozzle axis has to be defined to approximate the thermodynamic and kinematic properties (Fig.2).

Knowing $\bar{u}(\bar{x}, \bar{y}, \gamma)$ and $\bar{v}(\bar{x}, \bar{y}, \gamma)$, it is possible to determine two typical lines at the throat:

- the sonic line defined by: $\bar{u}^2 + \bar{v}^2 = 1$
- the line of the throat where $\bar{v} = 0$

Each point of ξ_0 has to be supersonic. Thus, ξ_0 is usually defined by a line starting from the line of throat. This point can be evaluated by the ratio $\bar{R}/\overline{H_t}$ where $\bar{R}$ is the curvature of the streamline on the line of the throat (see Fig.1) given by (13):

$$\frac{1}{\bar{R}} = \frac{\partial}{\partial \bar{x}}\left(\frac{\bar{v}}{\bar{u}}\right) = \frac{1}{\bar{u}}\left(\frac{\partial \bar{v}}{\partial \bar{x}}\right)_{\bar{v}=0} \qquad (13)$$

To ensure a smooth evolution of flow, this ratio is equal to 10. The β ratio is then defined by $\beta = \overline{H_t}/H_t$. The axis point is defined arbitrarily as $M = 1.1$ and its coordinates are calculated by reorganizing (12). ξ_0 is then discretized into $N = 20$ points and replaced in the dimensional system, and all thermodynamic properties are calculated according to the isentropic relations. Fig. 3 shows an example of ξ_0 in the normalized system.

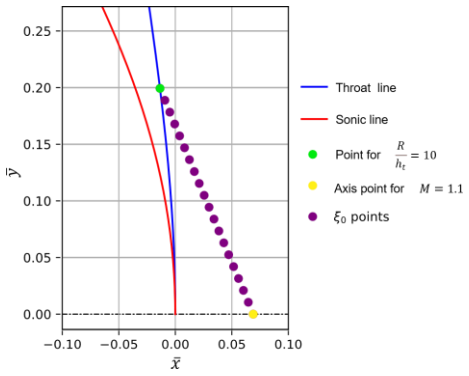

Fig. 3: Typical initial characteristic ξ_0 for $N = 20$ in the normalized system

The pressure evolution $p(x)$ is cropped to agree with the location of axis point of ξ_0 and then discretized in 50 points with a quadratic distribution (more point density closed to

the throat). Thermodynamic properties are evaluated in the same way as for ξ_0. This discretization provides a good compromise between computation time and the fineness of the calculated nozzle wall.

Procedure to calculate the solution

Each point $P_{i,j}$ (see Fig.2) is calculated by solving the system of equations (14) and (15) providing by the right- and left-running characteristics lines depending on the initial data:

$$\nu_{ij}(M,\gamma) - \varphi_{ij} = \nu_{i-1,j}(M,\gamma) - \varphi_{i-1,j} = cst = K_L \quad (14)$$

$$\nu_{ij}(M,\gamma) + \varphi_{ij} = \nu_{i,j-1}(M,\gamma) + \varphi_{i,j-1} = cst = K_R \quad (15)$$

This system provides $\nu_{ij}(M,\gamma)$ and φ_{ij}. $\nu_{ij}(M,\gamma)$ is used with the inverse function of (5) to calculate $M_{i,j}$. Then, for each point $P_{i,j}$, all the thermodynamic properties are evaluated with isentropic relations. Coordinates of point $P_{i,j}$ are calculated from the intersection of slopes of left-running and right-running characteristics respectively from $P_{i-1,j}$ and $P_{i,j-1}$ defined by (2). The points of the nozzle wall are evaluated along each right-running characteristic ξ_i by mass flow rate conservation with (16):

$$\dot{m}_{i,j} = \int_{Pi,0}^{Pi,j} \rho \cdot a \cdot d\xi \quad (16)$$

When $\dot{m}_{i,j} > \dot{m}_t$, a linear interpolation of ρ and a is done between $P_{i,j}$ and $P_{i,j-1}$ to adjust the mass flow rate to $\dot{m}_t$.

2.7 Method of Characteristics for Equivalent Gas Model

The MOC for the equivalent gas follows the same structure as the previous procedure but includes real gas effects through an equivalent heat capacity ratio model [Bufi 2016]. The CO_2 is assumed as a polytropic transformation obtained by the following equation:

$$\frac{p}{\rho^{\gamma eq}} = \frac{p_t}{\rho_t^{\gamma eq}} \quad (17)$$

(17) is then linearized by the logarithmic relation (18):

$$\log\left(\frac{p}{p_t}\right) = \gamma eq \cdot \log\left(\frac{\rho}{\rho_t}\right) \quad (18)$$

p is evaluated on 200 points evenly distributed between p_t and p_e. Associated $\rho(p, s_t)$ are determined with CoolProp. γeq is computed with a linear regression using the least squares method regression of (18). Tab.1 shows the influence of pressure in supercritical inlet conditions on γeq compared to γ_{ideal}.

Tab. 1: Polytropic coefficient γ_{eq} for different inlet pressure. $T_0 = 200\ °C$, $p_e = 6\ bar$

γ_{ideal}	γeq		
/	$80\ bar$	$100\ bar$	$110\ bar$
1.286	1.267	1.269	1.270

With the aim of controlling $scCO_2$ expansion, $p_e > 6\ bar$ will be advised to stay above the triple point of CO_2 ($p_{triple} = 5.1\ bar$ and $T_{triple} = -56.4\ °C$). Direct formation of dry ice from gas is thus avoided.

2.8 Advanced Gas Model (AGM)

In scenarios involving complex real gas effects of CO_2, nonlinear equations of state (EOS) prevent analytical integration of the governing equations. To address this, the numerical procedure inspired by [Bufi 2016] is employed, leveraging a method of characteristics (MOC) developed previously.

To initiate the procedure, the following points are executed:

- $\dot{m}_t$,$p(x)$ and thermodynamic properties at the throat are evaluated knowing (p_0, T_0) (section 2.4).
- Static enthalpy along the axis $h(x)$ is determined with CoolProp as $h(x) = h(p(x), s_t)$.
- Thermodynamics properties $\rho(x), T(x)$ and $a(x)$ along the axis are computed with CoolProp knowing $(p(x), s_t)$ and preservation of total enthalpy allows to write $V(x) = \sqrt{2[h_0 - h(x)]}$. $M(x)$ is then determined with $\big(a(x), V(x)\big)$.
- ξ_0 is calculated with the initialization procedure of (section 2.6) with γeq.

(2) and (3) are numerically integrated by a Euler corrector algorithm with iteration as described by [Bufi 2016]. The discretization is done along each characteristic line ξ_i and (3) is carried out by the finite-difference scheme (19):

$$A'\big(V_{ij} - V_{i,j-1}\big) \pm \big(\phi_{ij} - \phi_{i,j-1}\big) = 0 \quad (19)$$

Where $A = \sqrt{M^2 - 1}/V$ and $A' = (A_{ij} - A_{i,j-1})/2$. The predictor-corrector scheme used for computing compressible flow variables is divided into three steps. The following points present them briefly. n represent the number of iterations. More details are available in [Bufi 2016].

- *Predictor step:* Initialization with $V_{ij}(n) = V_{i,j-1}$ and $\varphi_{ij}(n) = \varphi_{i,j-1}$. Static flow quantities are evaluated with the conservation of total enthalpy and the isentropic expansion. New $P_{ij}(n)$ coordinates are then calculated.
- *Corrector step:* Coefficients A'_{ij} along right- and left-running characteristics are interpolated. Then a linear system in the two unknowns $V_{ij}(n+1)$ and $\varphi_{ij}(n+1)$ is solved using Cramer's rule.
- *Convergence Check:* The solution is accepted if:

$$\big|V_{ij}(n+1) - V_{ij}(n)\big| < \varepsilon \text{ and } \big|\varphi_{ij}(n+1) - \varphi_{ij}(n)\big| < \varepsilon \quad (20)$$

Where ε is a pre-set accuracy threshold fixed at 10^{-8}.

The calculation of wall points is carried out by mass flow conservation as presented previously.

3 RESULTS

An example of a 2D nozzle design with the three solver methods for supercritical inlet conditions is presented in this section. The input parameters are provided in Tab.2.

Tab. 2: Inlet parameters

p_0	T_0	p_e
$110\ bar$	$200\ °C$	$6\ bar$

This example enables an expansion of a single-phase gas within the nozzle, allowing the evaluation using CoolProp. For multiphase expansions, such as liquid–gas flows, the proportion of liquid and gas phases must be known in order to accurately compute the thermodynamic properties. The outlet pressure p_e allows staying above the triple point and getting as close as possible to atmospheric pressure in order to achieve an optimized design without pressure fluctuation. Here, the end of the nozzle wall is defined when the Mach number on the wall reaches $M_e = 2.55$ to ensure no more variations of fluid properties. Fig.4 shows the nozzle geometry obtained with the AGM solver.

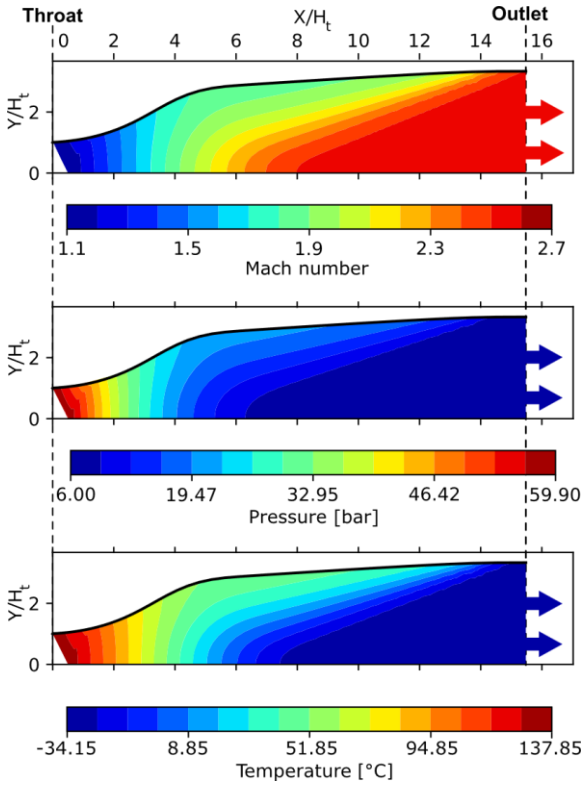

Fig. 4: Mach number, pressure and temperature surface for AGM in the divergent part. Axes are normalized with H_t

Fig.5. compares the divergent shape for each model. Ideal Gas Model and Equivalent Gas Model are similar due to the small variation of the heat capacity ratio. For the AGM, the consideration of real gas effects drastically modifies the thermodynamic properties of calculated points P_{ij}, resulting in a more important expansion ratio of the beginning of the divergent shape. Similar work on the design of nozzles for $ScCO_2$ has yielded similar results [Restrepo 2022].

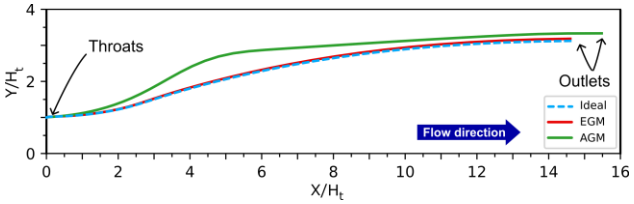

Fig. 5: Divergent shape for the three models. Axes are normalized with semi-height H_t

4 EXPERIMENTAL SETUP

A 2D jet facility has been developed to study the structure of CO_2 jets for liquid and supercritical conditions, as illustrated on Fig.6. The 2D nozzle profile is manufactured by wire EDM from a 1 mm thick steel shim. It consists of a stabilization chamber, which ensures the upstream conditions (p_0, T_0) before the converging section of the C-D part. It is clamped between two borosilicate glass plates, each approximately 25 mm thick. The jet expands into the environment, and grooves in the external structure let the jet freely in the plane. (X, Y). The free jet expansion can be observed in a $88\ mm$ by $32\ mm$ area, and the flow through the C-D-shape can be observed in a $10\ mm$ by $5\ mm$ area. The fluid is delivered by a custom-built system designed for delivering liquid and $scCO_2$ [Koulekpa 2022].

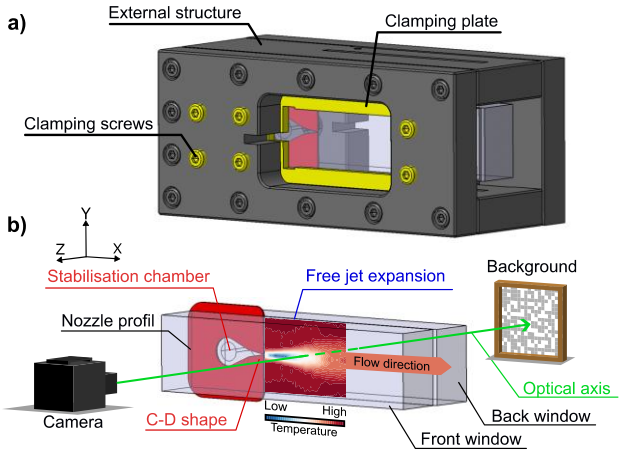

Fig. 6: a) Schematic of 2D jet facility and b) example of BOS setup to measure temperature gradient

Fig.7 presents an example of a CO_2 jet that was observed during preliminary tests with a high-speed camera, with the experimental setup to visualize it. Schlieren and shadowgraph techniques will be implemented in order to visualize the change of refractive indices or light intensity in a non-intrusive way [Settles 2001]. [Koulekpa 2025] used the Background Oriented Schlieren (BOS) method to measure the density and temperature gradient of an axisymmetric CO_2 orifice jet. The same method will be applied to characterize the jet structure of the designed nozzles, and Fig.6.a shows the setup constituted of a high-speed camera and a dotted background to perform the BOS measurement in 2D flow.

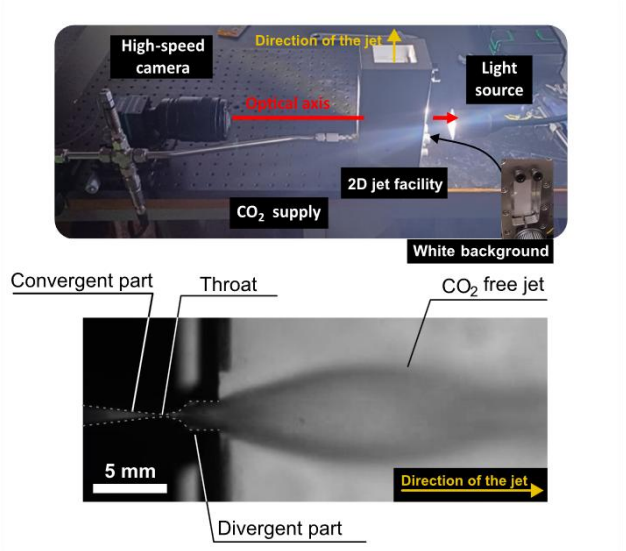

Fig. 7: Preliminary test for grayscale visualization of a CO_2 jet in liquid inlet condition: $p_0 = 80\ bar, T_0 = 20°C$, $H_t = 0.2\ mm$

5 SUMMARY

In the present work, the Method of Characteristics (MOC) was developed for ideal gases, equivalent gases (EGM), and an advanced real gas model (AGM) to design the divergent section of a De Laval nozzle. The main steps of the numerical implementation were translated into a code, and a design example was provided for supercritical CO_2 inlet conditions. The current modeling approach is restricted to single-phase gas expansion within the nozzle. A future version of the code will extend to include two-phase

expansions, enabling exploration of a new range of inlet conditions (p_0, T_0) closer to the critical point.

Implementation into Computational Fluid Dynamics (CFD) models is also planned, in order to compare the gradient of thermodynamics properties and to include the boundary layers effect [Chen 2023]. A 2D jet facility was presented and will be used in future experiments to assess temperature gradients and jet structure in a planar flow with Schlieren and shadowgraph techniques. It will also allow for the evaluation of phase changes during nozzle expansion.

Revolution-shaped micro-nozzles will be designed with the aim of integrating them into insert milling cutter bodies for machining operations using $ScCO_2$. Three nozzle outlet geometries will be tested to assess their impact on a grooving milling operation: a straight outlet, a conical outlet, and a curvilinear outlet designed using a numerical method tailored for axisymmetric flow (respectively illustrated in Fig.8). The main challenge lies in machining these micro-nozzle geometries into components that can be mounted on milling cutter bodies.

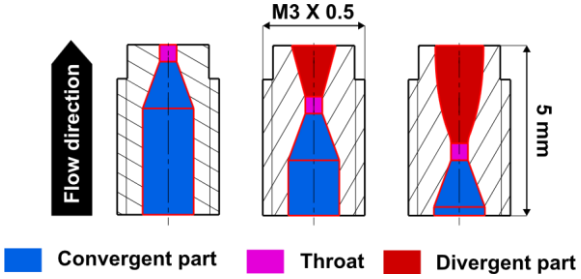

Fig.8: Example of micro-nozzle geometries: straight, conical, curvilinear divergent part

6 ACKNOWLEDGMENTS

The authors would like to thank the funders of this research work: SECO TOOLS, CONSTELLIUM.

7 REFERENCES

[Altharan 2024] Altharan, Y.M., Shamsudin, S., Al-Alimi, S., Saif, Y. and Zhou W. A review on solid-state recycling of aluminum machining chips and their morphology effect on recycled part quality, Heliyon, July 2024, Vol. 10, Issue 14 https://doi.org/10.1016/j.heliyon.2024.e34433

[Bell 2014] Bell, I.H., Wronski, J., Quoilin, S. and Lemort, V. Pure and Pseudo-pure Fluid Thermophysical Property Evaluation and the Open-Source Thermophysical Property Library CoolProp, Ind. Eng., January 2024, Chem. Vol. 53, Issue 6, pp 2498–2508. https://doi.org/10.1021/ie4033999

[Bufi 2016] Bufi E.A. Optimisation robuste de turbines pour les cycles organiques de Rankine (ORC). Arts et Métiers Institute of Technology, Politecnico di Bari. Dipartimento di Ingegneria Meccanica e Gestionale, 2016, tel-01535746

[Cai 2021] Cai, C., Liang, X., An, Q., Tao, Z., Ming, W. and Chen, M. Cooling/Lubrication Performance of Dry and Supercritical CO2-Based Minimum Quantity Lubrication in Peripheral Milling Ti-6Al-4V, Int. J. Precis. Eng. Manuf.-Green Technol., February 2003, Vol. 8, pp 405–421. https://doi.org/10.1007/s40684-020-00194-7

[Chen 2023] Chen, L., Deligant, M., Specklin, M. and Khelladi S. Validation and Application of HEM for Non-ideal Compressible Fluid Dynamic, Proceedings of the 4th International Seminar on Non-Ideal Compressible Fluid Dynamics for Propulsion and Power, Springer, May 2023, Cham, pp 156–165. https://doi.org/10.1007/978-3-031-30936-6_16

[Clarens 2006] Clarens, A.F., Hayes, K.F. and Skerlos, S.J. Feasibility of Metalworking Fluids Delivered in Supercritical Carbon Dioxide. J. Manuf. Process., 2006, Vol. 8, pp 47–53. https://doi.org/10.1016/S1526-6125(06)70101-3

[Délery 2010] Délery, J. Handbook of compressible aerodynamics. ISTE ; John Wiley, London, Hoboken, NJ., 2010

[Gao 2024] Gao, Z., Zhang, H., Ji, M., Zuo, C. and Zhang, J. Influence of Various Cooling and Lubrication Conditions on Tool Wear and Machining Quality in Milling Inconel 718. Int. J. Precis. Eng. Manuf.-Green Technol., September 2024, Vol. 11, pp 391–406. https://doi.org/10.1007/s40684-023-00558-9

[Huang 2022] Huang, H., Liu, S., Zhu, L., Qing, Z., Bao, H. and Liu, Z. Cooling and lubrication performance of supercritical CO2 mixed with nanofluid minimum quantity lubrication in turning Ti-6Al-4 V. Int. J. Adv. Manuf. Technol., January 2022, Vol. 122, pp 2927–2938. https://doi.org/10.1007/s00170-022-10091-9

[IATA, 2002] IATA Global Outlook for Air Transport - Sustained Recovery Amidst Strong Headwinds, 2022

[Koulekpa 2022] Koulekpa, K., Elias-Birembaux, H., Rossi, F. and Poulachon, G. Etude expérimentale de l'usinage du Ti6Al4V sous assistance CO2 supercritique, Manufacturing' 21 Conference, Paris-Saclay, October 2022 https://hal.science/hal-04011776

[Koulekpa 2025] Koulekpa, K. Développements expérimentaux pour l'analyse et l'optimisation de l'assistance CO2 supercritique en usinage. (phd thesis), Arts et Métiers Institute of Technology, 2025, tel-05127745

[Lettieri 2018] Lettieri, C., Paxson, D., Spakovszky, Z. and Bryanston-Cross, P. Characterization of Nonequilibrium Condensation of Supercritical Carbon Dioxide in a de Laval Nozzle, J. Eng. Gas Turbines Power, April 2018, Vol. 140, Issue 4, pp 041701. https://doi.org/10.1115/1.4038082

[Proud 2022] Proud, L., Tapoglou, N. and Slatter, T. A Review of CO2 Coolants for Sustainable Machining, Metals 12, February 2022, no.2, 283. https://doi.org/10.3390/met12020283

[Proud 2023] Proud, L., Tapoglou, N., Wika, K.K., Taylor, C.M. and Slatter, T. Role of CO2 cooling strategies in managing tool wear during the shoulder milling of grade 2 commercially pure titanium, Wear, March 2023, Vol. 524-525. https://doi.org/10.1016/j.wear.2023.204798

[Restrepo 2022] Restrepo, J.C., Bolaños-Acosta, A.F. and Simões-Moreira, J.R. Short nozzles design for real gas supersonic flow using the method of characteristics. Appl. Therm. Eng., May 2022, Vol. 207. https://doi.org/10.1016/j.applthermaleng.2022.118063

[Riquet 2011] Riquet, J.-P., Pelmard, P. and Verdier, J.-F. Method for recycling scrap containing aluminium-lithium-type alloys, Patent : EP1913166B1, 2011

[Settles 2001] Settles, G.S. Schlieren and Shadowgraph Techniques, Visualizing Phenomena in Transparent Media, Springer Berlin Heidelberg, 2001. https://doi.org/10.1007/978-3-642-56640-0

[Stephenson 2014] Stephenson, D.A., Skerlos, S.J., King, A.S. and Supekar, S.D. Rough turning Inconel 750 with supercritical CO2-based minimum quantity lubrication. J. Mater. Process. Technol., March 2014, Vol. 214, pp 673-680. https://doi.org/10.1016/j.jmatprotec.2013.10.003

[Tapoglou 2021] Tapoglou, N., Taylor, C. and Makris, C. Milling of aerospace alloys using supercritical CO2 assisted machining. Procedia CIRP, 2021, Vol. 101, pp 370–373. https://doi.org/10.1016/j.procir.2020.06.008